



Formation Flight of UAVs for Search and Detection Missions by Tracking Time-Variable Trajectories

Rolando Díaz-Castillo¹, Rosa Martha López-Gutiérrez^{1*}, Juan José Cetina-Denis² and César Cruz-Hernández²

¹ *Engineering, Architecture and Design Faculty, Baja California Autonomous University (UABC), Ensenada 22860, BC, México.*

² *Electronics and Telecommunication Department, Scientific Research and Advanced Studies Center of Ensenada (CICESE), Ensenada 22860, BC, México.*

Received: November 6, 2024; Revised: June 7, 2025

Abstract: In this paper, the formation problem of multiple unmanned aerial vehicles (UAVs) is addressed. In particular, the formation of UAVs is achieved by using complex systems theory and backstepping nonlinear control. We apply the obtained formation of multiple UAVs to search for and detect a target of interest within an exploration area. In addition, a coverage study of the formation of UAVs for search and detection by tracking time-variable trajectories is reported.

Keywords: *complex systems; formation control; backstepping control; multiple UAVs; search mission.*

Mathematics Subject Classification (2020): 70K42, 93-08, 93-16.

1 Introduction

From the formation of some kinds of birds to extend their flight time, to the grouping of fish to avoid attacks of predators, different groups of animals often associate naturally to achieve a common goal or benefit, which they individually could not achieve, and therefore could not survive [6], [18], [19].

The exchange of information due to the interactions between the members of these groups gives rise to a set of collective behaviors that are different from an isolated individual behavior. It is called emergent collective behavior [17], [21].

* Corresponding author: <mailto:roslopez@uabc.edu.mx>

In the literature, there are many works dealing with this problem, one of them is the work by R. Abas and Wu [1], in which the dynamic model of a quadcopter is studied by using the Newton-Euler method, and the synchronization of three quadcopters is achieved in the simulation using sliding modes as a control algorithm.

In the work done by P. Flores [9], the author faces the problem of the formation of a group of unmanned aerial vehicles (UAVs), for this a dynamic model of a quadcopter is considered using the Newton-Euler method, the control algorithm for the formation is backstepping control, and the formation of a group of three quadcopters is achieved.

In the work reported by A. Toledo [2], the dynamic model of a quadcopter is considered using the Newton-Euler method and an integral backstepping control algorithm with sliding modes is proposed for an unmanned aerial vehicle. The experimental results are obtained by using a Qball-X4 quadcopter.

In the work by N. Koksál [14], the dynamic model of the Qball-X4 quadcopter is considered. A PID control algorithm is used for the translation system and another algorithm is applied for the rotation system, the simulations results are obtained for a group of 3 quadcopters, and experimental tests with two Qball-X4 type quadcopters are carried out.

In the work done by X. Dong [7], a dynamic model for a small UAV type mini helicopter is considered assuming that there is a leading quadcopter and the other are followers, they use a PID control algorithm and obtain the formation of the group of quadcopters in simulation and experimental results.

The main goals of this paper are: (i) to obtain network synchronization and formation flight of coupled UAVs in star topology, considering a single master UAV with four slave UAVs. This objective is achieved by using recent results from complex systems theory. In addition, (ii) to apply the network formation to object detection, and (iii) to carry out a coverage study of the formation of UAVs for search and detection by tracking time-variable trajectories. To our knowledge, the results have not been reported.

The organization of the paper is as follows. In Section 2, the problem statement is presented. Section 3 describes the mathematical model of the UAV quadrotor used in this work. Section 4 contains the designed control algorithm for synchronization and formation of UAVs. Section 5 presents the obtained numerical results. In Section 6, an application to object detection is provided. Finally, some conclusions are given in Section 7.

2 Problem Statement

In recent decades, many control proposals have emerged in order to achieve formations in mobile robots. Particularly, formations in Unmanned Aerial Vehicles (UAVs) have received considerable interest due to their wide potential applications in the military, civil and industrial fields, and agriculture [10], [13]. The purpose of this study is to preserve mobility and compact groups at the same time, which generates advantages such as reduced implementation costs, increased robustness, system efficiency, etc.

The quadcopter is used to access hostile environments, where the safety of the pilots can not be guaranteed. The quadcopter's configuration makes it capable of taking off vertically, controlled landing, as well as great maneuverability. These advantages have attracted many researchers' interest in recent years.

Different control techniques can be applied to a quadcopter, for example, a nonlinear controller, PID control, backstepping, dynamic feedback linearization, and sliding modes,

among others. See for example [3], [7], [12].

The study of collective behaviors seen in nature and their representation in mathematical equations opens the door for multiple applications in robotics and, in our particular case, the formation of multiple unmanned aerial vehicles (UVAs).

The purpose of this paper is to reproduce collective behaviors observed in animals, namely synchronization and formation, and apply them to the networks of unmanned aerial vehicles (UVAs) for applications in search, rescue, and patrol task. Fig. 1 illustrates a group of quadcopters searching for the target of interest T.

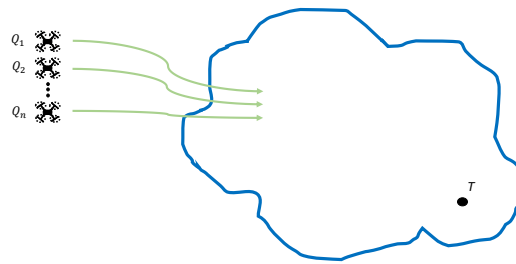


Figure 1: Group of quadrotors searching for the target T.

We will solve the stated problem on the network formation of five UAVs with a single master and four slaves by using complex systems theory and nonlinear backstepping control, providing an analytical stability proof based on the Lyapunov theory, and we will also analyze the search and detection coverage of the object in the area. In addition, for a particular type of UAV, we will use the mathematical model of the quadrotor described in Section 3.

3 Quadrotor Dynamic Model

The complete quadrotor dynamic model, with the x, y, z -plane position and orientation angles (*roll*, *pitch*, and *yaw*), is described by [2], [3]- [5], [20]

$$\begin{aligned}
 \ddot{\phi} &= \dot{\theta}\dot{\psi} \left(\frac{I_y - I_z}{I_x} \right) - \frac{J_r}{I_x} \dot{\theta}\Omega + \frac{l}{I_x} U_2, \\
 \ddot{\theta} &= \dot{\phi}\dot{\psi} \left(\frac{I_z - I_x}{I_y} \right) + \frac{J_r}{I_y} \dot{\phi}\Omega + \frac{l}{I_y} U_3, \\
 \ddot{\psi} &= \dot{\phi}\dot{\theta} \left(\frac{I_x - I_y}{I_z} \right) + \frac{l}{I_z} U_4, \\
 \ddot{x} &= (\cos\phi \sin\theta \cos\psi + \sin\phi \sin\psi) \frac{1}{m} U_1, \\
 \ddot{y} &= (\cos\phi \sin\theta \sin\psi - \sin\phi \cos\psi) \frac{1}{m} U_1, \\
 \ddot{z} &= -g + \cos\phi \cos\theta \frac{1}{m} U_1.
 \end{aligned} \tag{1}$$

The first three differential equations correspond to the quadrotor orientation $(\phi, \theta, \psi)^T$, and the last three differential equations represent the position of the quadrotor with respect to the original inertial frame $(x, y, z)^T$, see Figure 2.

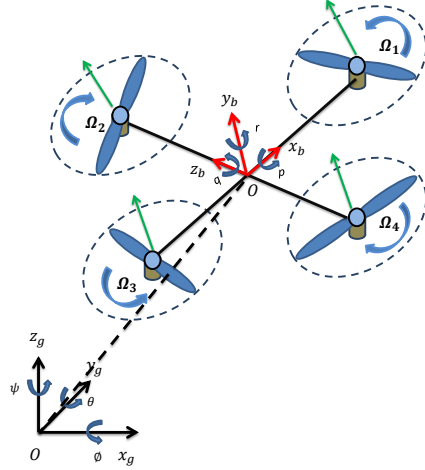


Figure 2: Quadcopter representation with respect to the inertial frame.

The angular velocity due to the propellers in each engine is represented by Ω_i , for $i = 1, 2, 3, 4$, respectively. The control inputs of the quadrotor are denoted by U_i , $i = 1, 2, 3, 4$, and Ω is a disturbance, which correspond to

$$\begin{aligned}
 U_1 &= b(\Omega_1^2 + \Omega_2^2 + \Omega_3^2 + \Omega_4^2), \\
 U_2 &= b(\Omega_4^2 - \Omega_2^2), \\
 U_3 &= b(\Omega_3^2 - \Omega_1^2), \\
 U_4 &= d(\Omega_2^2 + \Omega_4^2 - \Omega_1^2 - \Omega_3^2), \\
 \Omega &= \Omega_2 + \Omega_4 - \Omega_1 - \Omega_3.
 \end{aligned} \tag{2}$$

The quadrotor dynamic model described in Eq. (1) can be rewritten in a state space as $\dot{\mathbf{X}} = f(\mathbf{X}, \mathbf{U})$, introducing the following state vector:

$$\mathbf{X} = [\phi, \dot{\phi}, \theta, \dot{\theta}, \psi, \dot{\psi}, x, \dot{x}, y, \dot{y}, z, \dot{z}]^T, \tag{3}$$

where

$$\begin{aligned}
 x_1 &= \phi, & x_2 &= \dot{x}_1 = \dot{\phi}, \\
 x_3 &= \theta, & x_4 &= \dot{x}_3 = \dot{\theta}, \\
 x_5 &= \psi, & x_6 &= \dot{x}_5 = \dot{\psi}, \\
 x_7 &= z, & x_8 &= \dot{x}_7 = \dot{z}, \\
 x_9 &= x, & x_{10} &= \dot{x}_9 = \dot{x}, \\
 x_{11} &= y, & x_{12} &= \dot{x}_{11} = \dot{y}.
 \end{aligned} \tag{4}$$

From Equations (1) and (4), the quadrotor mathematical model can be described in

the state space as follows:

$$\dot{\mathbf{X}} = f(\mathbf{X}, \mathbf{U}) = \begin{pmatrix} x_2 \\ x_4x_6a_1 + x_4a_2\Omega + b_1U_2 \\ x_4 \\ x_2x_6a_3 + x_2a_4\Omega + b_2U_3 \\ x_6 \\ x_4x_2a_5 + b_3U_4 \\ x_8 \\ -g + (\cos x_1 \cos x_3) \frac{1}{m} U_1 \\ x_{10} \\ u_x \frac{1}{m} U_1 \\ x_{12} \\ u_y \frac{1}{m} U_1 \end{pmatrix}, \tag{5}$$

where

$$\begin{aligned} a_1 &= \frac{I_y - I_z}{I_x}, & a_2 &= -\frac{J_x}{I_x}, & a_3 &= \frac{I_z - I_x}{I_y}, & a_4 &= \frac{J_x}{I_y}, & a_5 &= \frac{I_x - I_y}{I_z}, \\ b_1 &= \frac{l}{I_x}, & b_2 &= \frac{l}{I_y}, & b_3 &= \frac{l}{I_z}, \\ u_x &= \cos x_1 \sin x_3 \cos x_5 + \sin x_1 \sin x_5, \\ u_y &= \cos x_1 \sin x_3 \sin x_5 - \sin x_1 \cos x_5. \end{aligned}$$

The quadrotor mathematical model (5) can be divided into two subsystems: orientation and translation. The first one is given by

$$\dot{\mathbf{x}}_o = \mathbf{f}_o(\mathbf{x}_i) + \mathbf{B}_i \mathbf{U}_{oi}, \tag{6}$$

where $\mathbf{U}_{oi} = (U_2 \ U_3 \ U_4)^T$,

$$\mathbf{f}_o = \begin{pmatrix} x_2 \\ x_4x_6a_1 + x_4a_2\Omega \\ x_4 \\ x_2x_6a_3 + x_2a_4\Omega \\ x_6 \\ x_4x_2a_5 \end{pmatrix}, \quad \mathbf{B}_i = \begin{pmatrix} 0 & 0 & 0 \\ b_1 & 0 & 0 \\ 0 & 0 & 0 \\ 0 & b_2 & 0 \\ 0 & 0 & 0 \\ 0 & 0 & b_3 \end{pmatrix}. \tag{7}$$

On the other hand, the translation subsystem is described by the following expression:

$$\dot{\mathbf{x}}_{ti} = \mathbf{f}_t(\mathbf{x}_i) + \mathbf{G} \mathbf{U}_{ti}, \tag{8}$$

where $\mathbf{U}_{ti} = (U_1 \ U_x \ U_y)^T$,

$$\mathbf{f}_t = \begin{pmatrix} x_8 \\ -g \\ x_{10} \\ 0 \\ x_{11} \\ 0 \end{pmatrix}, \quad \mathbf{G} = \begin{pmatrix} 0 & 0 & 0 \\ \frac{\cos x_1 \cos x_3}{m} & 0 & 0 \\ 0 & 0 & 0 \\ 0 & \frac{1}{m} & 0 \\ 0 & 0 & 0 \\ 0 & 0 & \frac{1}{m} \end{pmatrix}. \tag{9}$$

The physical parameters of the quadrotor mathematical model (5) are given in Table 1.

Parameter	Definition	Value
m	Mass	0.650 kg
I_x	x-axis inertia	$7.5e^{-3} \text{ kgm}^2$
I_y	y-axis inertia	$7.5e^{-3} \text{ kgm}^2$
I_z	z-axis inertia	$1.3e^{-2} \text{ kgm}^2$
b	Thrust coefficient	$3.13e^{-3} \text{ N s}^2$
d	Drag coefficient	$7.5e^{-7} \text{ Nms}^2$
J_r	Rotor inertia	$6e^{-5} \text{ kgm}^2$
l	Arm length	0.23 m
g	Gravity	9.8 N/kg

Table 1: Physical parameters of the quadrotor mathematical model (5).

4 Control Design for Trajectory Tracking

In nonlinear control theory, backstepping is a technique developed around 1990 by Petar V. Kokotovic, Miroslav Krstiv, and Ioannis Kanellakopoulos [15] to design stabilizing controls for a special class of nonlinear dynamical systems. These systems are built from subsystems that originate from an irreducible subsystem that can be stabilized using some other method.

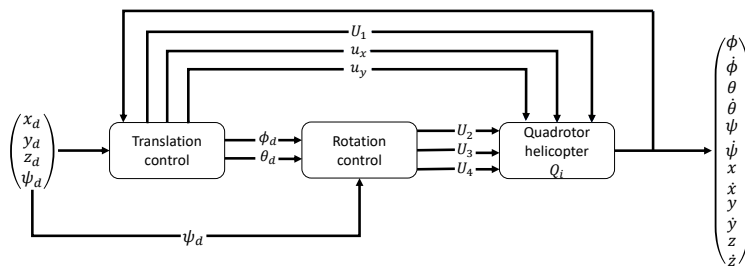


Figure 3: Block diagram of quadrotor helicopter Q and its controller.

In the backstepping approach, the control law is designed so that the system can follow the desired trajectory. For this, it is considered that the quadrotor mathematical model (5) can be divided into two subsystems, one is the orientation and the other is the

position [5], as previously discussed in Section 3. Figure 3 shows the block diagram of quadcopter and its controller for tracking a desired path.

Due to its complete independence with respect to the other subsystem (Eqs.(6) and (8)), the control input for the angular rotations of the subsystem is considered first and then the position control input is derived. A desired trajectory x_{1d} is defined, in which the following error is given by

$$z_1 := x_{1d} - x_1, \quad (10)$$

from expression (10), we have

$$\dot{z}_1 = \dot{x}_{1d} - \dot{x}_1. \quad (11)$$

From the quadrotor mathematical model (5), $\dot{x}_1 = x_2$ is known. Substituting into (11), we have

$$\dot{z}_1 = \dot{x}_{1d} - x_2. \quad (12)$$

Now, consider the following Lyapunov candidate function in terms of z_1 :

$$V(z_1) = \frac{1}{2}z_1^2. \quad (13)$$

Differentiating the candidate Lyapunov function with respect to time gives

$$\dot{V}(z_1) = z_1\dot{z}_1. \quad (14)$$

Substituting Equation (12) in (14) gives

$$\dot{V}(z_1) = z_1(\dot{x}_{1d} - x_2). \quad (15)$$

x_2 is considered as a virtual control to stabilize z_1 , thus we have

$$x_2 = \dot{x}_{1d} + \alpha_1 z_1, \quad (16)$$

we make $\alpha_1 > 0$ so that the derivative of the Lyapunov function is negative definite. Solving for (16) in (15), we have

$$\begin{aligned} \dot{V}(z_1) &= z_1(\dot{x}_{1d} - x_2) \\ &= z_1(\dot{x}_{1d} - \dot{x}_{1d} - \alpha_1 z_1) \\ &= -\alpha_1 z_1^2. \end{aligned} \quad (17)$$

After the variable change

$$z_2 = x_2 - \dot{x}_{1d} - \alpha_1 z_1, \quad (18)$$

differentiating Equation (18), we have

$$\dot{z}_2 = \dot{x}_2 - \ddot{x}_{1d} - \alpha_1 \dot{z}_1. \quad (19)$$

The following Lyapunov candidate function is proposed as a function of (z_1, z_2) :

$$V(z_1, z_2) = \frac{1}{2}(z_1^2 + z_2^2). \quad (20)$$

Differentiating the candidate Lyapunov function and solving, we have

$$\begin{aligned}\dot{V}(z_1, z_2) &= z_2 \dot{z}_2 + z_1 \dot{z}_1 \\ &= z_2(\dot{x}_2 - \ddot{x}_{1d} - \alpha_1 \dot{z}_1) + z_1(\dot{x}_{1d} - x_2) \\ &= z_2(\dot{x}_2 - \ddot{x}_{1d} - \alpha_1(\dot{x}_{1d} - x_2)) + z_1(\dot{x}_{1d} - x_2).\end{aligned}\quad (21)$$

Solve x_2 from Equation (18): $x_2 = z_2 + \dot{x}_{1d} + \alpha_1 z_1$, thus

$$\begin{aligned}\dot{V}(z_1, z_2) &= z_2(\dot{x}_2 - \ddot{x}_{1d} - \alpha_1(\dot{x}_{1d} - x_2)) + z_1(\dot{x}_{1d} - x_2) \\ &= z_2(\dot{x}_2 - \ddot{x}_{1d} - \alpha_1(\dot{x}_{1d} - (z_2 + \dot{x}_{1d} \\ &\quad + \alpha_1 z_1))) + z_1(\dot{x}_{1d} - (z_2 + \dot{x}_{1d} + \alpha_1 z_1)) \\ &= z_2 \dot{x}_2 - z_2(\ddot{x}_{1d} - \alpha_1(z_2 + \alpha_1 z_1)) - z_1 z_2 - \alpha_1 z_1^2 \\ &= z_2(a_1 x_4 x_6 + a_2 x_4 \Omega + b_1 U_2) - z_2(\ddot{x}_{1d} - \alpha_1(z_2 + \alpha_1 z_1)) \\ &\quad - z_1 z_2 - \alpha_1 z_1^2.\end{aligned}\quad (22)$$

Considering $\ddot{x}_{1d,2d,3d} = 0$ and given $\dot{V}(z_1, z_2) < 0$, the virtual controller U_2 is designed as

$$U_2 = \frac{1}{b_1}(z_1 - a_1 x_4 x_6 - a_2 x_4 \Omega - \alpha_1(z_2 + \alpha_1 z_1) - \alpha_2 z_2).\quad (23)$$

The remaining control inputs U_3 , U_4 , and U_1 can be solved by a similar approach, obtaining the corresponding virtual controllers for each control input:

$$U_3 = \frac{1}{b_2}(z_3 - a_3 x_2 x_6 - a_4 x_2 \Omega - \alpha_3(z_4 + \alpha_3 z_3) - \alpha_4 z_4),\quad (24)$$

$$U_4 = \frac{1}{b_3}(z_5 - a_5 x_2 x_4 - \alpha_5(z_2 + \alpha_1 z_1) - \alpha_6 z_6).\quad (25)$$

The control input for the positioning subsystem is given by

$$U_1 = \frac{m}{\cos x_1 \cos x_3}(z_7 + g - \alpha_7(z_8 + \alpha_7 z_7) - \alpha_8 z_8 + \ddot{x}_7),\quad (26)$$

$$u_x = \frac{m}{U_1}(z_9 - \alpha_9(z_{10} + \alpha_9 z_9) - \alpha_{10} z_{10} + \ddot{x}_9),\quad (27)$$

$$u_y = \frac{m}{U_1}(z_{11} - \alpha_{11}(z_{12} + \alpha_{11} z_{11}) - \alpha_{12} z_{12} + \ddot{x}_{11}),\quad (28)$$

where

$$\begin{aligned}z_1 &= x_{1d} - x_1, \\ z_2 &= x_2 - \dot{x}_{1d} - \alpha_1 z_1, \\ z_3 &= x_{3d} - x_3, \\ z_4 &= x_4 - \dot{x}_{3d} - \alpha_3 z_3, \\ z_5 &= x_{5d} - x_5, \\ z_6 &= x_6 - \dot{x}_{5d} - \alpha_5 z_5, \\ z_7 &= x_{7d} - x_7, \\ z_8 &= x_8 - \dot{x}_{7d} - \alpha_7 z_7, \\ z_9 &= x_{9d} - x_9, \\ z_{10} &= x_{10} - \dot{x}_{9d} - \alpha_9 z_9, \\ z_{11} &= x_{11d} - x_{11}, \\ z_{12} &= x_{12} - \dot{x}_{11d} - \alpha_{11} z_{11}.\end{aligned}\quad (29)$$

Communication in a multi-agent topology can be represented directly or indirectly by a graph, where each node is an agent and the edges are the communication media that exist between them [11]. A group of 5 quadcopters (Eq.(5)) is considered, one of which is the master quadrotor (M) and the rest are slave quadrotors (S_1, S_2, S_3, S_4). The network of quadrotors can be represented by the following graph shown in Figure 4.

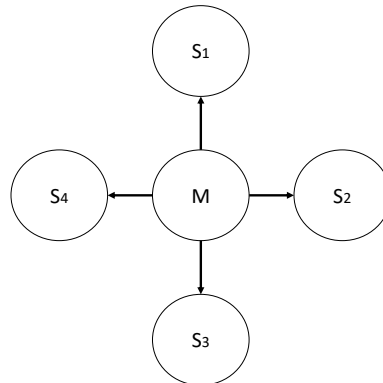


Figure 4: Connection graph of 5 quadrotors.

The corresponding adjacency matrix associated with this graph is

$$A(G) = \begin{pmatrix} 0 & 0 & 0 & 0 & 0 \\ 1 & 0 & 0 & 0 & 0 \\ 1 & 0 & 0 & 0 & 0 \\ 1 & 0 & 0 & 0 & 0 \\ 1 & 0 & 0 & 0 & 0 \end{pmatrix}. \tag{30}$$

The network synchronization was achieved through the variables z_i of the control law, given by Eq. (29), so each slave quadrotor $S_i, i = 1, 2, 3, 4$, follows the master quadrotor M , and their states will have to follow the states of the master quadrotor. The auxiliary variables for each quadrotor are given as follows:

$$\begin{aligned} z_{1S_i} &= x_{1M} - x_{1S_i}, \\ z_{2S_i} &= x_{2S_i} - \dot{x}_{1M} - \alpha_{1S_i} z_{1S_i}, \\ z_{3S_i} &= x_{3M} - x_{3S_i}, \\ z_{4S_i} &= x_{4S_i} - \dot{x}_{3M} - \alpha_{3S_i} z_{3S_i}, \\ z_{5S_i} &= x_{5M} - x_{5S_i}, \\ z_{6S_i} &= x_{6S_i} - \dot{x}_{5M} - \alpha_{5S_i} z_{5S_i}, \\ z_{7S_i} &= x_{7M} - x_{7S_i}, \\ z_{8S_i} &= x_{8S_i} - \dot{x}_{7M} - \alpha_{7S_i} z_{7S_i}, \\ z_{9S_i} &= x_{9M} - x_{9S_i}, \\ z_{10S_i} &= x_{10S_i} - \dot{x}_{9M} - \alpha_{9S_i} z_{9S_i}, \\ z_{11S_i} &= x_{11M} - x_{11S_i}, \\ z_{12S_i} &= x_{12S_i} - \dot{x}_{11M} - \alpha_{11S_i} z_{11S_i}. \end{aligned} \tag{31}$$

When performing the calculations from Equation (5) to Equation (9), with the help of the auxiliary variables (31), the following control inputs for network synchronization

of the quadrotors in star connection are obtained:

$$U_{1l} = \frac{m}{\cos\phi\cos\theta}(\dot{x}_8 + g) + \frac{m}{\cos\phi\cos\theta} \sum_{j=1}^{N=4} a_{ij}[(1 + \alpha_7\alpha_8)(x_{7j} - x_{7i}) + (\alpha_7 + \alpha_8)(x_{8j} - x_{8i})], \quad (32)$$

$$u_{xl} = \frac{m}{U_{1l}}\dot{x}_{10} + \frac{m}{U_{1l}} \sum_{j=1}^{N=4} a_{ij}[(1 + \alpha_9\alpha_{10})(x_{9j} - x_{9i}) + (\alpha_9 + \alpha_{10})(x_{10j} - x_{10i})], \quad (33)$$

$$u_{yl} = \frac{m}{U_{1l}}\dot{x}_{12} + \frac{m}{U_{1l}} \sum_{j=1}^{N=4} a_{ij}[(1 + \alpha_{11}\alpha_{12})(x_{11j} - x_{11i}) + (\alpha_{11} + \alpha_{12})(x_{12j} - x_{12i})], \quad (34)$$

where $(l = 1, 2, 3, 4)$ is the i -th quadrotor, $(\dot{x}_8, \dot{x}_{10}, \dot{x}_{12})$ are the states of the master quadrotor M, a_{ij} are the entries of the adjacency matrix (30) associated with the graph used for communication between the quadrotors.

In order to achieve quadrotor formation, the use of a vector Δ with components corresponding to each axis is proposed and then used in the controller of each slave quadrotor (S_i , $i = 1, 2, 3, 4$). This vector separates each slave from the master M by a distance corresponding to each axis in the plane (x, y, z) . The auxiliary variables for the formation of each quadrotor respectively are given as follows:

$$\begin{aligned} z_{1S_i} &= x_{1M} - x_{1S_i}, \\ z_{2S_i} &= x_{2S_i} - \dot{x}_{1M} - \alpha_{1S_i}z_{1S_i}, \\ z_{3S_i} &= x_{3M} - x_{3S_i}, \\ z_{4S_i} &= x_{4S_i} - \dot{x}_{3M} - \alpha_{3S_i}z_{3S_i}, \\ z_{5S_i} &= x_{5M} - x_{5S_i}, \\ z_{6S_i} &= x_{6S_i} - \dot{x}_{5M} - \alpha_{5S_i}z_{5S_i}, \\ z_{7S_i} &= x_{7M} - x_{7S_i} + \Delta_{zS_i}, \\ z_{8S_i} &= x_{8S_i} - \dot{x}_{7M} - \alpha_{7S_i}z_{7S_i}, \\ z_{9S_i} &= x_{9M} - x_{9S_i} + \Delta_{xS_i}, \\ z_{10S_i} &= x_{10S_i} - \dot{x}_{9M} - \alpha_{9S_i}z_{9S_i}, \\ z_{11S_i} &= x_{11M} - x_{11S_i} + \Delta_{yS_i}, \\ z_{12S_i} &= x_{12S_i} - \dot{x}_{11M} - \alpha_{11S_i}z_{11S_i}. \end{aligned} \quad (35)$$

5 Numerical Results

When considering a star-shaped topology connection between five quadrotors, a numerical simulation is carried out, in which the group of quadrotors will follow a desired circular trajectory with a radius of 3 meters at a height of 2 meters. These trajectories start after the quadrotors takes off. The initial conditions for the quadrotors are: Master $(x_1(0), y_1(0), z_1(0)) = (0, 0, 0)$, slave 1 $(x_2(0), y_2(0), z_2(0)) = (0.5, 0, 0)$, slave 2 $(x_3(0), y_3(0), z_3(0)) = (-0.5, 0, 0)$, slave 3 $(x_4(0), y_4(0), z_4(0)) = (1.5, 0, 0)$, and slave 4 $(x_5(0), y_5(0), z_5(0)) = (-1.5, 0, 0)$. The physical parameters of the five quadrotors are taken from Table 1 and the alphas are definitely positive with a value of 50.

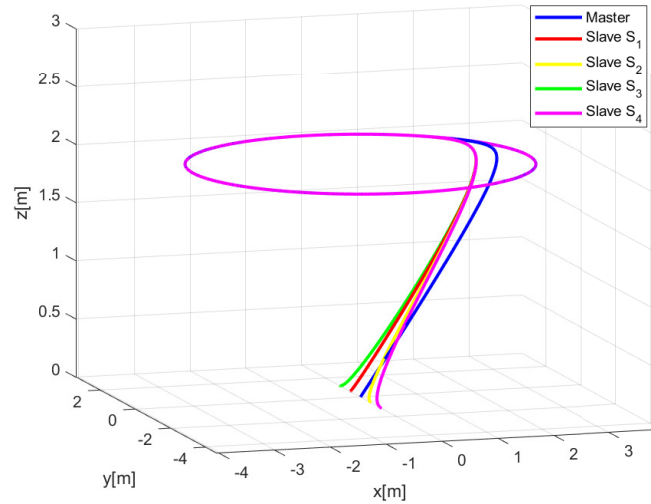


Figure 5: Synchronization of five quadrotors to a desired circular trajectory.

In Figure 5, it can be seen that the network of five quadrotors is synchronized in a desired circular trajectory. Next, to achieve the network formation of five quadrotors, we proceed to give a net constant separation between the master quadrotor M and the slave quadrotors S_i by using the vector Δ for the separation. The initial conditions for quadrotors are the same as considered in the previous simulation. The quadrotors are separated by a distance Δ on the x -axis for a horizontal line formation, where the slave quadrotors S_1 and S_2 are desired to be separated by a distance $D1 = 0.5\text{ m}$ from the master M , while slave quadrotors S_3 and S_4 are separated from the master quadrotor M by a distance $D2 = 1\text{ m}$. This can be seen in Figure 6.

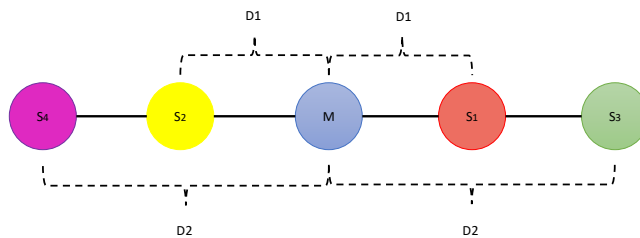


Figure 6: Separation Δ for the formation of five quadrotors.

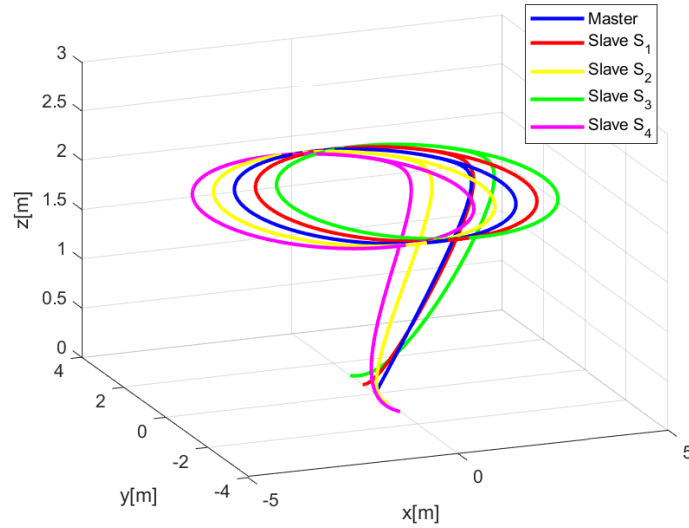


Figure 7: Flight of the formation of five quadrotors describing a circular trajectory.

Figure 7 shows the five quadrotors are already in formation describing a circular trajectory. Next, we will apply the formation of quadrotors to the search for an object on a surface. For this, a rectangular search surface is considered, but it can be deduced that using a circular trajectory to explore a rectangular surface would have a great disadvantage since there are unexplored areas since the object, when placed randomly on the surface, could not be detected. For this reason, it is decided to use the Lissajous trajectories, of which the denser trajectory is used.

6 Application to Object Detection

The target of interest to be detected within the search area is a circle object, which varies in size with respect to the total percentage of the search area. The target to be searched and detected is randomly placed within the exploration area. The target can be considered detected by using the coordinates of the quadrotors and the coordinates where the center of the target is located, considering the radius of the target. The detection of the target is determined by using the coordinates of the trajectories of each quadrotor and the coordinates of the center of the target calculating their distances by means of the expression

$$d(A, B) = |\overrightarrow{AB}|. \quad (36)$$

Substituting the coordinates of the center of the target and the trajectory of the quadrotor, the elements of vector A and B are obtained. The distance is calculated as follows:

$$d(A, B) = |\overrightarrow{AB}| = \sqrt{(X_2 - X_1)^2 + (Y_2 - Y_1)^2}, \quad (37)$$

where X_2 and Y_2 are the quadrotor coordinates, and X_1 and Y_1 are the position of the center of the target. The following Figure 8 shows how the detection is done.

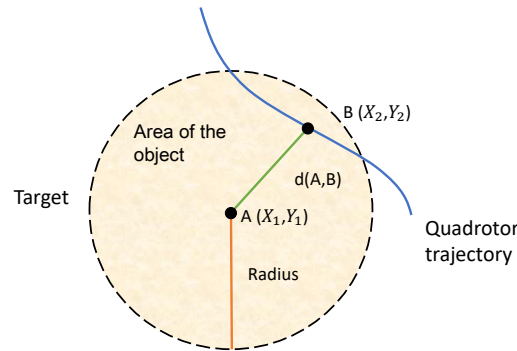


Figure 8: Target detection process.

For target detection, if any point of the trajectories of the quadrotors is within the radius of the target, it indicates that this point is within the area of the target, concluding that it was detected and, given that more than one quadrotor trajectory passes through this area, we can determine which quadrotor passed first and met this condition before the others.

Lissajous curves

The Lissajous curve, also known as the Lissajous figure or Bowditch curve, is the graph of the parametric equation system corresponding to the superposition of two simple harmonic motions in perpendicular directions [8], [16], [22] defined by

$$x = A\sin(w_x t + \alpha), \quad y = B\sin(w_y t + \beta), \quad \delta = \alpha - \beta. \tag{38}$$

The Lissajous curves for different parameter values are shown in Figure 9.

Now, we will proceed to carry out some numerical simulations in MatLab, where quadrotors formation explores a rectangular area. This search surface, or the area of exploration, has a dimension of 8x6 m², the Lissajous curve used has the parameter values 5 : 6 and $\frac{\pi}{2}$ with the values of A = 3, B = 3, w_x = 6, and w_y = 5. Quadrotors will be considered to start outside of this area. The search for the randomly placed target will begin, and then the area of this target will be varied as shown in Table 2.

The first simulation is carried out with a target size of 10% with respect to the search area and in the network, the quadrotors are separated by a distance Δ on the x-axis for a horizontal line formation, where the slave quadrotors S₁ and S₂ are desired to be separated by a distance D1 = 0.5 m from the master M, while the slave quadrotors S₃ and S₄ are separated from the master quadrotor M by a distance D2 = 1 m, as shown in Figure 6. The initial conditions for the quadrotors are: Master (x₁(0), y₁(0), z₁(0)) = (4.5, 0, 0), slave 1 (x₂(0), y₂(0), z₂(0)) = (4.5, 0.6, 0), slave 2 (x₃(0), y₃(0), z₃(0)) = (4.5, 1.2, 0), slave 3 (x₄(0), y₄(0), z₄(0)) = (4.5, -0.6, 0), and slave 4 (x₅(0), y₅(0), z₅(0)) = (4.5, -1.2, 0).

As seen in Figure 10, several trajectories of the quadrotor formation pass over the target, so it can be deduced that it was easily detected within the search surface. It can

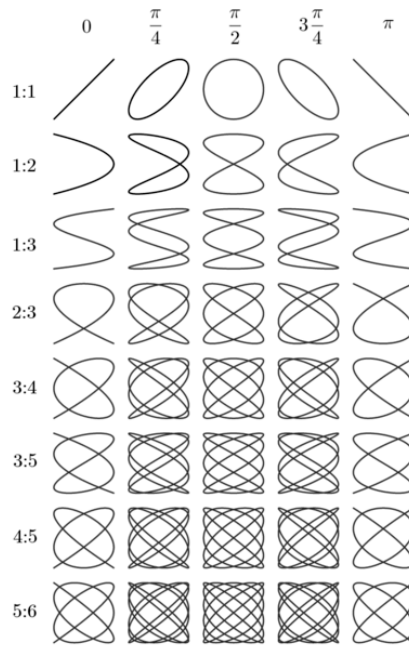


Figure 9: Lissajous curves described by (38) for different parameter values.

Surface percentage	Object area	Object radius
10 %	4.8 m^2	1.23 m
7.5 %	3.6 m^2	1.07 m
5 %	2.4 m^2	0.87 m
1 %	0.48 m^2	0.39 m
0.5 %	0.24 m^2	0.27 m
0.3 %	0.144 m^2	0.21 m
0.1 %	0.048 m^2	0.12 m
0.01 %	0.0048 m^2	0.039 m

Table 2: Object area table.

be considered that the searched target was detected due to its big size, so it is decided to reduce it, according to Table 2. Next, a new numerical simulation is performed using a target with a size of 1% with respect to the rectangular search surface. The initial conditions for quadrotors are the same as considered in the previous simulation.

Figure 11 shows that the searched target was detected by at least two quadrotors. Considering that its size makes it easier to be found, its dimensions can be reduced further with respect to the rectangular search surface.

In addition, another simulation is performed now using a target sized 0.1% with respect to the rectangular search surface. The initial conditions for quadrotors are the

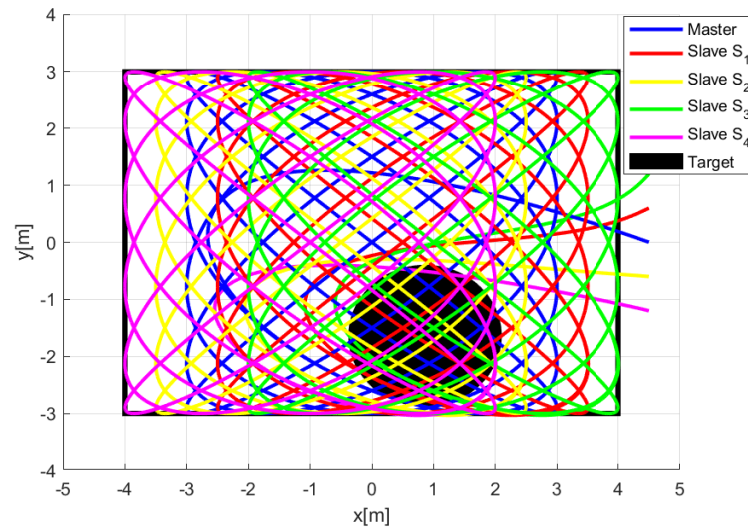


Figure 10: Search for a target sized 10% of the exploration area.

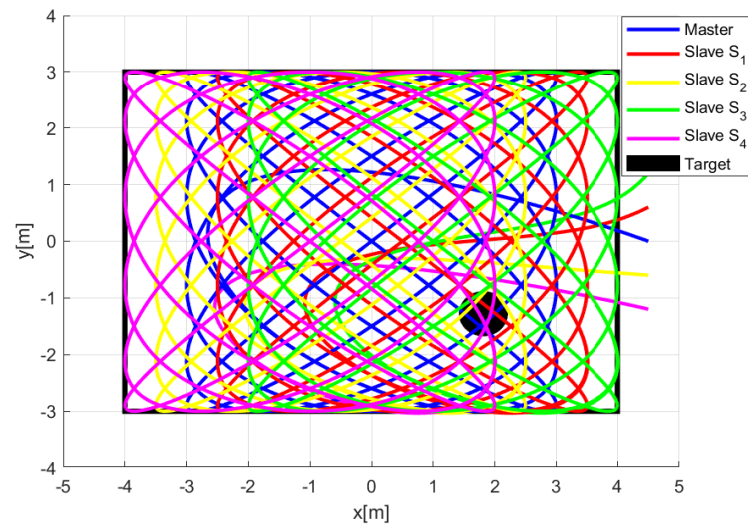


Figure 11: Search for a target sized 1% of the exploration area.

same as considered in the previous simulation.

Figure 12 shows that the target was detected by two of the slave quadrotors. In addition, it can be considered that it already has a suitable size with respect to the rectangular search surface, therefore we will use this target size. It was decided to use this target size to run 10 tests, to determine if some of the quadrotors can detect it. The

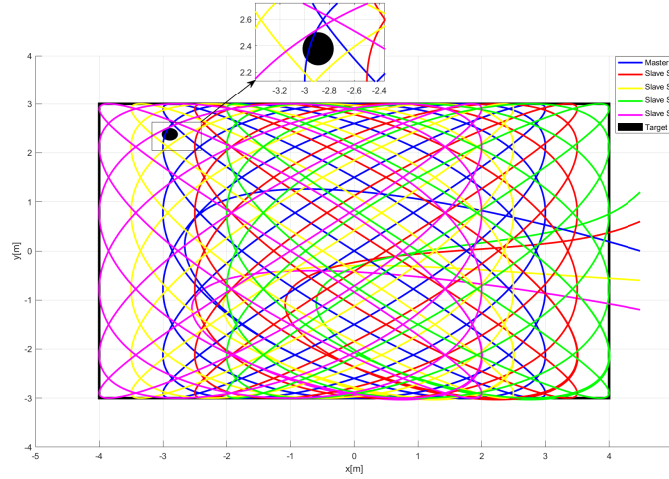


Figure 12: Search for a target sized 0.1% of the exploration area.

obtained numerical results are shown in Table 3.

Test	Run time	Detection time	x-axis position	y-axis position	Target detected by
1	0.622 s	966.648 s	2.439 m	2.334 m	S_1
2	0.624 s	389.48 s	-2.891 m	2.334 m	M
3	0.620 s	309.201 s	1.026 m	-2.315 m	M
4	0.620 s	309.201 s	-1.717 m	0.269 m	S_3
5	0.631 s	958.754 s	3.546 m	2.674 m	S_1
6	0.626 s	147.690 s	-2.654 m	-2.707 m	S_2
7	0.629 s	250.066 s	2.328 m	-2.060 m	M
8	0.628 s	128.67 s	-0.606 m	2.391 m	S_3
9	0.630 s	1047.094 s	2.265 m	2.643 m	S_2
10	0.736 s	72.773 s	1.207 m	-2.670 m	S_3

Table 3: 10 tests to search for a target sized 0.1 % of the rectangular search area.

As shown in Table 3, the target was detected in each of the ten tests that were carried out. However, considering the size of the target in Figure 12, it can be seen that there are zones through which no trajectory passes and the target could be located in any of them. For this reason, it was decided to combine some of the Lissajous curves of the Figure 9 to get a suitable trajectory for the formation of quadrotors that do pass through these zones.

6.1 Lissajous curves as desired trajectories

It is desired to explore most of the search area, for which some of the Lissajous curves will be used. First, the curve with the parameters 2 : 3 and $\frac{\pi}{2}$ will be used. Taking

into account that, due to the shape of the curve, there will be unexplored zones, it is decided to combine it with another Lissajous curve with the parameters 3 : 4 and $\frac{\pi}{2}$. These curves can be seen in Figure 9.

Considering the combined trajectory 1 with two mentioned Lissajous curves, one after another, we have

$$Trajectory_1 = \begin{cases} t_0 & \text{to } t_1; & x = 3\sin(2\pi t + \pi), & y = 3\sin(3\pi t + 0.5\pi), \\ t_1 & \text{to } t_2; & x = 3\sin(4\pi t + \pi), & y = 3\sin(3\pi t + 0.5\pi). \end{cases} \quad (39)$$

To explore the rectangular search area with the combined $trajectory_1$, the final trajectory is taken into consideration. With the combination of both trajectories, a target with the size 0.1 % of the total search area will be detected. This is shown in Figure 13.

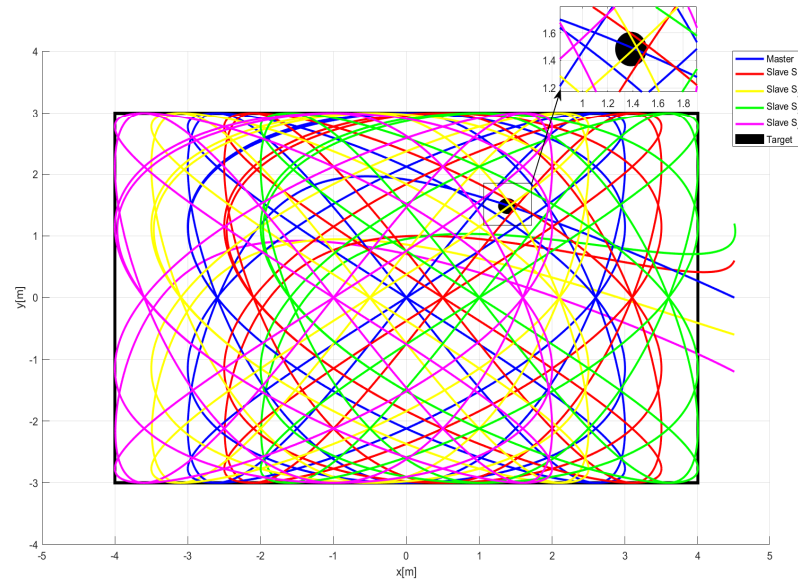


Figure 13: Target search with the combined trajectory 1 for the target sized 0.1% of the rectangular search area.

Ten tests are performed with this combined trajectory 1 for target detection, the numerical results are shown in Table 4.

According to the obtained results (Table 4), the target was also found with this combined trajectory 1. However, the unexplored zones did not decrease. Therefore, it was decided to use another combination of two other Lissajous curves.

We explore the search area again, making use of a different combination of the Lissajous curves. The curve with the parameters 3 : 4 and $\frac{\pi}{2}$ will be first used, and then another curve with parameters 6 : 5 and $\frac{\pi}{2}$. These curves can be seen in Figure 9.

The resulting combined trajectory 2 is described as follows.

$$Trajectory_2 = \begin{cases} t_0 & \text{to } t_1; & x = 3\sin(4\pi t + \pi), & y = 3\sin(3\pi t + 0.5\pi), \\ t_1 & \text{to } t_2; & x = 3\sin(6\pi t + \pi), & y = 3\sin(5\pi t + 0.5\pi). \end{cases} \quad (40)$$

The resulting search $trajectory_2$ is shown in Figure 14.

Test	Run time	Detection time	x-axis position	y-axis position	Target detected by
1	1.044 s	865.115 s	2.439 m	2.334 m	S_2
2	0.519 s	792.091 s	-2.891 m	2.334 m	M
3	0.157 s	1075.385 s	1.026 m	-2.315 m	S_2
4	0.145 s	60.001 s	-1.717 m	0.269 m	S_1
5	0.146 s	286.197 s	3.546 m	2.674 m	S_1
6	0.148 s	834.347 s	-2.654 m	-2.707 m	S_2
7	0.155 s	1142.108 s	2.328 m	-2.060 m	S_3
8	0.136 s	888.934 s	-0.606 m	2.391 m	S_3
9	0.141 s	2215.229 s	2.265 m	2.643 m	S_3
10	0.128 s	454.929 s	1.207 m	-2.670 m	S_1

Table 4: Test results for combined trajectory 1 for the search of the target sized 0.1% of the rectangular search area.

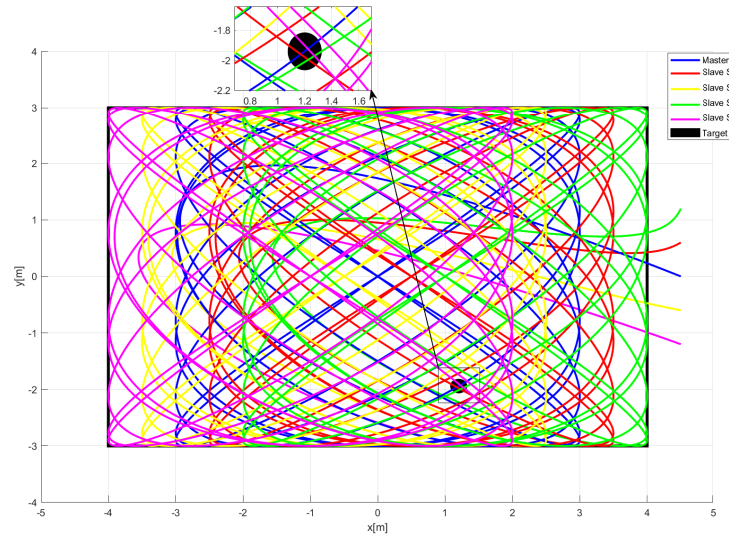


Figure 14: Target search with the combined trajectory 2 for a target sized 0.1% of the rectangular search area.

We perform ten tests with this combination for target detection and the results are shown in Table 5.

With the combined trajectory 2 of these two Lissajous curves, it is observed that some of the trajectories pass through the zones that they did not pass before (Figure 12); and the target was successfully detected in all ten tests, as shown in Table 5.

In the last table, only 10 of the 100 tests that were carried out were recorded, of which only in one case, the randomly placed target could not be detected.

The target search time is measured from the moment all five quadrotors start to fly

Test	Run time	Detection time	x-axis position	y-axis position	Target detected by
1	0.472 s	865.11 s	2.439 m	2.334 m	S_2
2	0.293 s	792.091 s	-2.891 m	2.334 m	M
3	0.154 s	1075.385 s	1.026 m	-2.315 m	S_2
4	0.140 s	60 s	-1.717 m	0.269 m	S_1
5	0.155 s	286.197 s	3.546 m	2.674 m	S_1
6	0.139 s	834.347 s	-2.654 m	-2.707 m	S_2
7	0.138 s	1142.108 s	2.328 m	-2.060 m	S_3
8	0.148 s	888.934 s	-0.606 m	2.391 m	S_3
9	0.152 s	2215.229 s	2.265 m	2.643 m	S_3
10	0.173 s	189.443 s	1.207 m	-2.670 m	M

Table 5: Test results for combined trajectory 2 for the search of the target sized 0.1% of the rectangular area.

and till the moment when any of them finds the object within the search area, as shown in Figure 15.

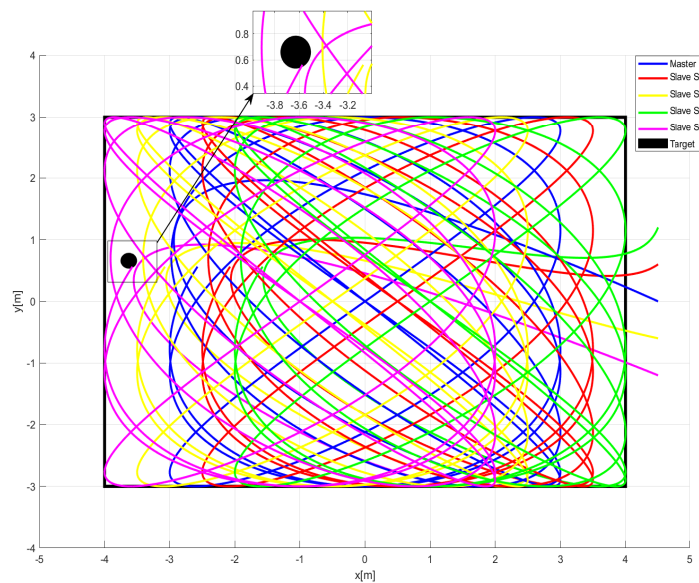


Figure 15: Target search and detection time for the formation of quadrotors.

Figure 15 shows that the target was detected by a slave quadrotor within the rectangular search area. The position of the center of the target was $(x, y) = (-3.628 \text{ m}, 0.659 \text{ m})$ and it was found in 12,877.043 seconds.

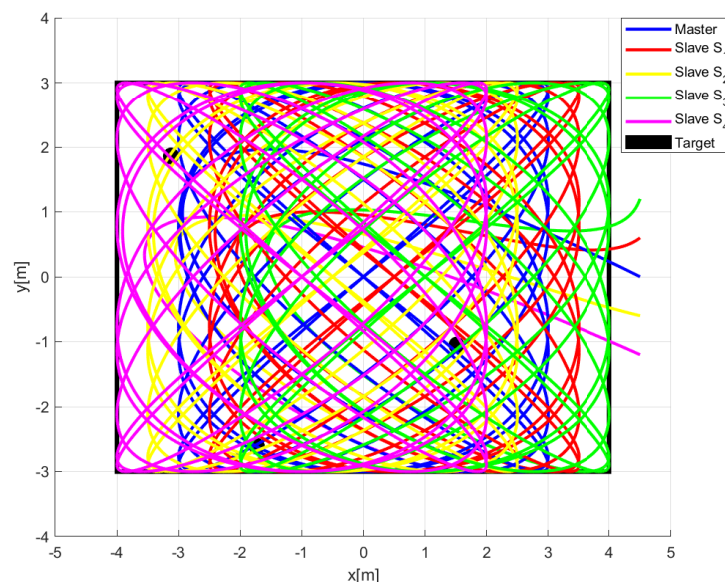


Figure 16: Three targets detected by the formation of quadrotors.

6.2 Three targets detection

In Figure 16, the detection of three targets placed randomly within the rectangular search surface is simulated and it is observed that at least one of the trajectories of the quadrotors passes through any of them, so it is assumed that they were detected.

In order to determine the percentage of the exploration area that is covered by the trajectories of the quadrotors formation, it is divided into 3136 squares of equal size and those that are visited by some quadrotor are noted, see Figure 17. The size of each square was determined to be smaller than the target to be detected. Using this method for both combinations of trajectories, a percentage of 84.27% of the covered area was obtained for the first case, and 92.12% for the second, demonstrating that the latter is more suitable for finding targets. With these results, it is concluded that the trajectories could easily find almost any targets in the rectangular search area, including small ones.

6.3 Discussion

The used exploration area is a rectangle which is 6 meters wide and 8 meters long. It is explored with the formation of five quadrotors. At first, they formed a vertical line and followed a desired circular trajectory, where it was observed that there were large unexplored zones. If none of the trajectories of the quadrotors passes over that zone, it is considered as not explored. Approximately 48% of the total search area remained unexplored, predominantly the central zone.

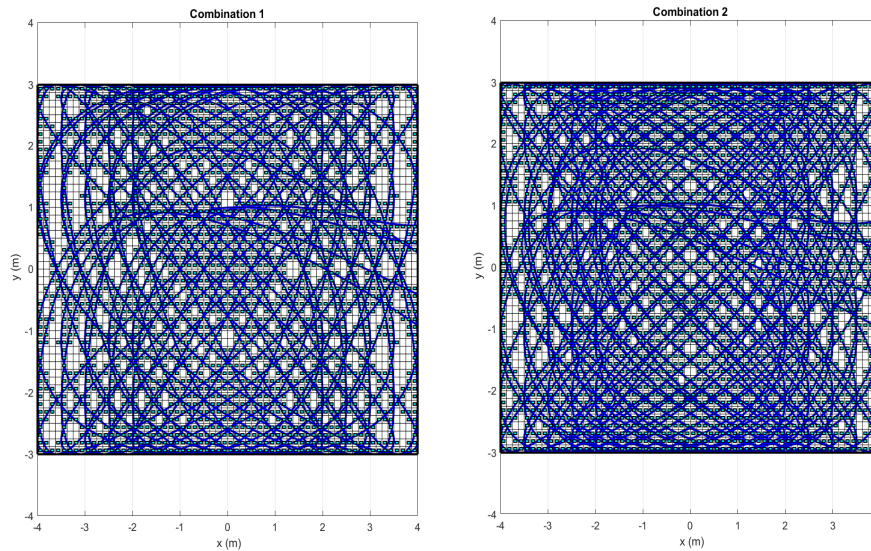


Figure 17: Quadcopters formation training trajectories coverage: a) by combined trajectory 1 and b) by combined trajectory 2.

Some tests were also carried out with other trajectories by using different parameters for the Lissajous curves, and it was observed that the unexplored zones were reduced. Different trajectories were made, taking the densest one, thus decreasing the unexplored zones between the quadrotors, with 4 % of the total unexplored surface.

Various formations were applied in the search and detection of the target. The first formation was a vertical line in which the slave quadrotors were observed to leave the boundaries of the search surface. The “V” formation was also used and it was observed that there were unexplored zones, mainly in the upper corners of the search surface. Therefore it was decided to use the formation in a horizontal line to explore this surface.

Next, the search surface was explored by using now two combinations of the Lissajous curves with different parameters. Ten tests for each combination were carried out. Because the target was found every time, another 90 tests were made (100 in total for each one). In the first case, comparing with the trajectory in Figure 13, an efficiency of 96% was reached. Exploring the search surface with the second combination, an efficiency of 99% was obtained.

7 Conclusions

In this paper, we have presented the formation problem of multiple UAVs for applications to search and detection by tracking time-variable trajectories. The main contributions of this work are: the mentioned formation was obtained by using complex systems theory and backstepping nonlinear control. We made a comprehensive study of UAVs formation coverage for search and detection of a random target within the search zone

by tracking time-variable trajectories. The reported numerical results show that the methodology employed meets the purpose of detecting the target within the search zone and reducing the unexplored zones by the combination of time-varying trajectories. Thus, in future work, we plan the physical implementation of the proposed formation scheme, we will use switching trajectories and switching topology connection, as well as chaotic trajectories.

Acknowledgment

This work was supported by CONAHCyT, México under Research Grand A1-S-31628.

References

- [1] R. Abbas and Q. Wu. Formation tracking for multiple quadrotor based on sliding mode and fixed communication topology. In: *2013 5th International Conference on Intelligent Human-Machine Systems and Cybernetics (IHMSC)* **2** (2013) 233–238.
- [2] M. E. Antonio-Toledo and E. N. Sanchez, A. Y. Alanis, J. A. Flórez and M. A. Perez-Cisneros. Real-time integral backstepping with sliding mode control for a quadrotor UAV. *IFAC-PapersOnLine* **13** (2018) 549–554.
- [3] S. Bouabdallah, P. Murrieri and R. Siegwart Design and control of an indoor micro quadrotor. In: *Robotics and Automation, 2004. Proceedings. ICRA '04 2004 IEEE International Conference on Robotics and Automation* **5** (2004) 4393–4398.
- [4] S. Bouabdallah and R. Siegwart. Backstepping and sliding-mode techniques applied to an indoor micro quadrotor. In: *Robotics and Automation, 2005. ICRA 2005 Proceedings of the 2005 IEEE International Conference on Robotics and Automation* (2005) 2247–2252.
- [5] S. Bouabdallah. *Design and Control of Quadrotors with Application to Autonomous Flying*. Ecole Polytechnique Federale de Lausanne, Lausana, 2007.
- [6] I.D. Couzin, J. Krause, R. James, G. D. Ruxton and N. R. Franks. Collective memory and spatial sorting in animal groups. *Journal of Theoretical Biology* **218** (2002) 1–11.
- [7] Xi. Dong and Y. Zhou, Z. Ren and Y. Zhong. Time-varying formation tracking for second-order multi-agent systems subjected to switching topologies with application to quadrotor formation flying. *IEEE Transactions on Industrial Electronics* **64** (2017) 5014–5024.
- [8] J. Flemming and A. Hornes. Lissajous-like figures with triangular and square waves. *Revista Brasileira de Ensino de Física* **35** (2013) 3702.
- [9] P. P. Flores, P. Castillo and F. Castanos. Backstepping-Based Controller for Flight Formation. In: *2019 International Conference on Unmanned Aircraft Systems (ICUAS)* (2017) 263–269.
- [10] P. K. Freeman and R. S. Freeland. Agricultural UAVs in the US: potential, policy and hype. *Remote Sensing Applications: Society and Environment* **2** (2015) 35–43.
- [11] C. Godsil and G. F. Royle. *Algebraic Graph Theory*. Springer Science & Business Media, **207**, 2001.
- [12] D. Ivanov, I. Kalyaev and S. Kapustyan. Method of circles for solving formation task in a group of quadrotor UAVs. In: *Systems and Informatics (ICSAI), 2014 2nd International Conference on Systems and Informatics* (2014) 236–240.
- [13] A. King. Technology: The future of agriculture. *Nature* **544** (2017) S21–S23.
- [14] N. Koksal, B. Fidan and K. Buyukkabasakal. Real-time implementation of decentralized adaptive formation control on multi-quadrotor systems. In: *European Control Conference (ECC), IEEE* (2015) 3162–3167.

- [15] M. Krstic, I. Kanellakopoulos and P. V. Kokotovic. *Nonlinear and Adaptive Control Design*. Wiley, 1995.
- [16] J. D. Lawrence. *A Catalog of Special Plane Curves*. Courier Corporation, 2013.
- [17] Q. Ouyang, Z. Wu, Y. Cong and Z. Wang. Formation control of unmanned aerial vehicle swarms: A comprehensive review. *Asian Journal of Control* (2023) **25** 570–593.
- [18] D.J. Sumpter. The principles of collective animal behaviour. *Philosophical Transactions of the Royal Society B: Biological Sciences* (2006) **361** 5–22.
- [19] D.J. Sumpter. *Collective Animal Behavior*. Princeton University Press, 2010.
- [20] A. Swarup and Sudhir. Comparison of Quadrotor Performance Using Backstepping and Sliding Mode Control. In: *International Conference on Circuits, Systems and Control* **1** (2014) 79–82.
- [21] T. Han, M. Chi, Z. Guan, B. Hu, J. Xiao and Y. Huang. Distributed three-dimensional formation containment control of multiple unmanned aerial vehicle systems. *Asian Journal of Control* **19** (2017) 1103–1113.
- [22] S. T. Thornton and J. B. Marion. *Classical Dynamics of Particles and Systems*. Cengage Learning, 2021.